THE EFFECTS OF THE TRANSIENT AND PERFORMANCE LOSS RATES ON PV OUTPUT PERFORMANCE

Chibuisi C. Okorieimoh
School of Electrical & Electronic Engineering
Dublin Energy Lab
Technological University Dublin
Dublin, Ireland
chibuisi.okorieimoh@tudublin.ie

Brian Norton
School of Electrical & Electronic Engineering
Dublin Energy Lab
Technological University Dublin
Dublin, Ireland
brian.norton@tudublin.ie

Michael Conlon
School of Electrical & Electronic Engineering
Dublin Energy Lab
Technological University Dublin
Dublin, Ireland
michael.conlon@tudublin.ie

Abstract

Solar photovoltaic (PV) panels experience long-term performance degradation as compared to their initial performance, resulting in lower like-per-like efficiencies and performance ratios. Manufacturers of solar photovoltaic modules normally guarantee a lifespan of more than 20 years. To meet such commitments, it is important to monitor and mitigate PV module degradation during this period, as well as beyond, to recognize maintenance and repair needs. Solar PV modules degrade over time, becoming less effective, less reliable, and eventually unusable. The effects of transient and performance loss rates on the output performance of polycrystalline silicon (p-Si) solar PV modules are the focus of this study. PV modules' electrical performance and solar energy conversion efficiency change as solar irradiance and ambient temperature change. A rise in ambient temperature or a decrease in solar irradiance, for example, all result in a reduction in performance.

Large variations in operating conditions due to uncontrollable external parameters such as cloud movement and wind velocity, as well as changes in factors external to PV systems such as unexpected shading, inverter problems, and control failures, may trigger transient performance changes on PV modules output. The data used in this analysis were from the Warrenpoint site location of the Electric Supply Board (ESB) for the years 2016-2020. Clear days in winter, spring, summer, and autumn were caused by a rise in daily sunshine hours in February, May, June, and September, according to the output performance. Due to the highest amount of solar irradiation at the site location, these days saw an increase in PV output generation. According to the performance loss rates, the median degradation rates in 2016 (4.5%/year to 14%/year) and 2017 (0.1%/year to 5.2%/year) are 8.40%/year and 3.87%/year, respectively. This means that the degradation rate is greater than 1%/year, the hazardous probability is between 90% and 100%, and a severity of 10 is given (With an associated failure of corrosion in solder bonds). 2018 (-7.5%/year to 2.5%/year), 2019 (-16%/year to -23%/year), and 2020 (-5.1%/year to -10% /year) had median degradation rates of -2.75%/year, -18.23%/year, and -5.2%/year, respectively. This shows that the degradation rates are less than 1% per year, and their hazardous probabilities range from severity rank 9 to 1, or 80% to 70% to 0% safety risk. All of these factors have a negative impact on PV output performance.

Keywords: *Transient, Performance loss rates, PV output performance, Degradation rates.*

INTRODUCTION

Solar PV panels experience long-term performance degradation resulting in lower like-per-like efficiency and performance ratios when compared with their initial performance [1]. Also, there are some transient effects (such as PV ambient temperature, wind velocity, shade, and dust particles) that reduce the output performance of the solar PV panels [2]. Reducing rates of PV module degradation aims to maintain the efficiency of solar PV systems [3]. As manufacturers usually guarantee the life span of PV modules for more than 20 years [3], it is, therefore, necessary to track and mitigate the degradation of PV modules over this period both during and beyond this period knowing degradation behavior is essential for operation, maintenance, and repair [1]. Most significantly, many PV module failures and, performance losses are caused by the gradual accumulation of damaged PV modules due to long-term outdoor exposure in harsh environments. This outdoor environmental stress is known as weathering [4]. To put a check on the outdoor installed PV modules, there is a need for accelerated tests. Outdoor testing of PV modules may take a longer time to be accomplished and it is impossible to wait up to 20-25 years to introduce a new PV module. Hence, it is important to develop and use accelerated tests to quantify or measure up the new PV modules [5]. Such accelerated stress tests are thermal cycling, humidity-freeze, damp heat, mechanical load (both static and dynamic), and ultraviolet exposure [5]. When a PV module fails to generate power, such failure will be seen as a reliability issue while a decrease in output of a PV module is caused by environmental degradation such as corrosion and it is classified as a durability issue. Therefore, the durability and reliability issues may eventually lead to PV module failure [4].

IEECP'21, July 29-30, 2021, Silicon Valley, San Francisco, CA – USA

DAI : https://sci-index.com/DAI/2021.99101/IEECP/14736087

A. PV Durability and Reliability Issues

The best way to deal with the PV reliability issues is by the use of the bathtub reliability curve (see Figures 1 (a) and 1 (b)) to find the physics of failure for each mode [6]. The bathtub reliability curve of a PV module is a graphical model made to represent the failure rate of a group of PV modules over some time. The curve helps the PV manufacturers to predict when failures occur on the PV module and possibly identify the root causes of the failure and possible ways of preventing them [4]. The bathtub reliability curve describes the failure rate of the PV module as a function of in-service life. Therefore, the curve consists of three essential parts, namely: Failure mode A (infant mortality), failure mode C (normal life), and failure mode B (end of life wear-out).

Failure mode A: Failure mode A is the early life failure (also, known as infant mortality) that normally occurs in the first 1-2 years of a PV module's life. Failure mode A occurs at the initial stage of the module's life cycle. The cause of failure mode A may be due to fundamental design faults, processing issues, errors in manufacturing, or inappropriate installation [4]. Therefore, Passing IEC 61215 or 61646 qualification tests are not proof that a PV module has been tested and shown to be durable and reliable rather the IEC environmental stress test protocols are designed primarily to test the period of early life failures (infant mortality) (see Figure 1 (b)) [6].

Failure mode C: Failure mode C is the constant (random) failures (also, known as normal life). This is the second part of the failure mode that occurs within the lifespan of the PV module. It is called the "constant (random) failures" because the failures in this mode are usually predictable and homogeneous. This failure mode usually occurs within this period when the stresses of the module have exceeded the strength of its weakest component. The cause of this failure mode is a result of unexpected environmental stress or load issues. For instance, when a PV module exceeds its capabilities it can suffer from a normal life failure (failure mode C).

Failure mode B: Failure mode B is the last part of the curve known as the end of life for the PV module (also, known as the end of life wear-out). In this failure mode, the curve rises steeply as many of the PV modules simply reach the point where they failed due to simple age or wear and tear. Failures of this kind are reasonably predictable.

B. Distinguishing Transient Performance changes from longer-term degradation

PV module output varies with solar irradiance and module temperature. It is also affected by shading, rain, and dust [7],[8]. All these variations are transient on a variety of timescales and/or reversible. Degradation refers to the loss of output due to physical degradation or damage to the PV cell, the effects are not reversible [1]. It refers to effects that will ultimately require the replacement of a PV cell for the system to return to its initial performance. The transient effect caused by an increase in PV cell ambient temperature can lead to reductions in output and efficiencies [2]. Degradation is measured by changes in mean efficiency and/or performance ratio over the long term as illustrated indicatively in Figure 2 [1]. It can also be observed in perturbation caused by cell failure in the current-voltage (I-V) curves for an array [1].

Individual module degradation can be attributed to intrinsic property changes in the PV materials caused by external effects such as:

- Potential induced degradation (PID) [9]; and
- Light-induced degradation (LID) [10].

The outdoor operation of cells as part of a module in an array means mechanisms external to the solar cell such as corrosion in interconnections and solder bonds play a significant role in performance degradation [3]. This makes it important to determine the degradation rates under outdoor operational conditions rather than indoor testing of isolated modules. [3], classified the major difficulties in evaluating degradation rates of PV modules from real operational data into:

- Large fluctuations of the operational data due to uncontrollable external parameters such as weather conditions like solar radiation, rain, cloud movement, wind velocity, and ambient temperature together with unexpected changes of factors external to PV systems such as unexpected shading, inverter problems, and control failures.
- systematic 'degradation' in the measurement of PV module operational performance caused by control sensor drifting with time as a result of electronic aging of components such as the drifting of irradiance sensors. The energy output of a PV system depends on weather conditions [11], [12], [3]. The degradation rate of silicon PV modules is around -0.7% per year of maximum power rating [11]. Reducing rates of PV module degradation aim to maintain the efficiency of solar PV systems [3]. As manufacturers usually guarantee the life span of PV modules for more than 20 years [3], it is, therefore, necessary to track and mitigate the degradation of PV modules over this period. Both during and beyond this period knowing degradation behavior is essential for operation, maintenance and repair.

C. Degradation Rates of Photovoltaic Modules

The study of annual degradation rates of recent crystalline silicon PV modules was carried out by Tetsuyuki and Atsushi [13]. Six crystalline silicon PV modules connected to an electric power grid were analyzed. Three indicators were used for the annual degradation rates of the different crystalline silicon PV: energy yield, performance ratio, and indoor power. The performance of the module was evaluated from electricity output measurements taken over 3 years. The following trends were found in the three indicators; energy yield: 0.0, -0.4% per year, 0.0, 0.1% per year, 1.5% per year and 0.5% per year, performance ratio: 0.0, -0.4% per year, -0.1% per year, 0.0, 1.4% per year and 0.5% per year and indoor power: 0.1% per year, -0.3% per year, 0.2% per year, 0.0, 0.7% per year and 0.6% per year were similar. The performance of the newly installed PV modules was found to decrease by over 2% as a result of initial light-induced degradation (LID) after installation [13].

The power output of an outdoor PV module has been shown to reduce as a result of thermal cycling causing crack formation between solders and metals [14]. Dunlop and Halton [7] studied the degradation of PV modules in outdoor conditions for 22 years. They monitored the electrical power outputs of monocrystalline silicon (m-Si), polycrystalline silicon (p-Si), and amorphous silicon (a-Si) modules. They found an 8% to 12% decrease in maximum power output of the PV modules (P_{max}) after 20 years of outdoor exposure. Their research showed that about 80% of the reduction was due to corrosion and the remaining 20% was attributed to dust accumulating on the PV modules. An experimental study of degradation modes and their effects on the PV module was conducted after 12 years of field operation [15]. Their investigation found that degradation led to annual reductions in output power ranging between 2.08% and 5.2%. Short circuit current (I_{sc}) is reduced by between 2.75% and 2.84% annually. The open-circuit voltage (V_{oc}) was found to be the least affected, with annual reductions ranging between 0.01% and 4.25%. The existence of only one highly degraded PV module in a PV system reduces daily output from Takatoshi et al, [16]:

i. 19.8 kWh to 18.7 kWh during sunny days;
ii. 11.3 kWh to 10.8 kWh during partly cloudy sunny days; and
iii. 5.5 kWh to 5.3 kWh during cloudy days.

D. Analysis of Risk Priority Number (RPN) on the Severity of PV Failure Modes

Failure Modes and Effects Analysis (FMEA) finds the effect of each failure mode and its causes on the system, according to the severity (S), occurrence (O), and detect-ability (D) [17]. The IEC 60812 standard has assumed a different range of S, O, and D for a PV system, which is helpful to identify the particular single failure mode based on RPN for the particular PV system and operating environment conditions [17]. A measurement of RPN is therefore expressed in (1) [17]:

$$RPN = S \times O \times D \quad (1)$$

Where:
S is the severity, which is a non-dimensional number. Severity determines the single failure mode, which strongly affects the PV system performance.
O is the occurrence, which depends on the probability of occurrence of a defect in the PV system during the exposure time.
D is the detection, which technology or instrument can identify the failure modes in a PV system during its exposure time.
The severity rank of failure mode depends on the degradation rate per year and safety issues. It is very difficult to find out the severity rank of a particular failure mode, as the degradation of a PV module is a cumulative sum of many factors [18],[19]. The highest rank in the severity given according to the safety issue probably insulation resistance failure, de-lamination, and burn mark occurs in the PV module, it is a threat or hazard to person or either property [17]. The severity number from 9 to 10 related to safety issues and the highest degradation factor, whereas the numbers from 8 to 1 depending on the performance degradation factor. In the present study, the severity rank performs according to References [20],[21]. The rank of severity has been given by Pramod et al [17] in Table 1.

MATERIALS AND METHODS

A. Site Location and Climate Description

The location chosen for this study is based on the Electricity Supply Board ESB) site located at Upper Dromore Road, Warrenpoint, Northern Ireland at 54.115551°N latitude and 6.263654°W longitude. The City of Warrenpoint acquires its power from the ESB public grid, which is shared with other residential and industrial consumers.
(https://www.google.com/maps/place/Newry+BT34+3PN,+UK/@54.1132142,-6.2642131,248a,35y,44.92t/data=!3m1!1e3!4m5!3m4!1s0x4860da664698253b:0xd3507b57cb2eea3!8m2!3d54.1150048!4d-6.2630492)is used to identify the site location.

B. System Monitoring and Data Acquisition

The data acquisition system used in this research consists of two SMA STP-20000TL-30 inverters each with a 20 W sensor box and a data logger. The sensor box measures the total solar radiation on the solar PV modules in-plane. The sensor box and the inverter have been connected to the data logger and the power injector. The data recording was set at 15 minutes (quarter-hour) intervals in the data logger and was extracted directly from the Excel spreadsheets to the computer and then analyzed using the MATLAB and Excel software tools.

RESULTS

A. Transient (Partial Shading) Effect in Solar Cells

I. Description of System

In this study, a system description of distributed circuit simulations of a PV module under partial shading conditions is presented. The PV module is connected to a variable DC voltage source converter (VSC) to quantify the I-V and P-V characteristics curves. A MATLAB SIMULINK is used to model the circuit: (i) as three strings of 20 series-connected cells parallel to bypass diodes which allow current flow when cells are shaded or damaged with a standard irradiance of 1 kWm^{-2} applied to String 1 (cells 1-20) while (ii) partial shading is applied to String 2 (cells 21-40) with an irradiance of 0.3 kWm^{-2} and (iii) String 3 (cells 41-60) with an irradiance of 0.6 kWm^{-2} as shown in Figure 4.

II. Simulation Process

The model is therefore simulated and at the end of the simulation, the I-V and P-V characteristics curves were plotted. When the PV module is connected to the voltage-sourced converter (VSC) it makes it difficult for the Maximum Power Point Tracking (MPPT) algorithm to converge at the highest peak. The global maximum power point (GMPP) indicated in the red circle of Figure 5 is 334 W at the maximum current of 5.29 A. The resultant characteristics of the PV array are shown in Figure 5. The P-V curves generate three peaks under partially shaded conditions (see Figure 5).

III. Simulation Results

Figure 6 shows the variation in the solar PV cell string and bypass diode used to reduce the shading effect. In string 1 (i.e., cells 1-20), the bypass diode (with blue color) has zero current. This is because string 1 solar cells do not have any shading effects. While in String 2 (i.e., 21-40 cells) and String 3 (i.e., 41-60 cells) solar cells had shading effects. It is noticed that the current flow is above zero. This shows that the bypass diode works.

B. Inverter Percentage Conversion Loss

When the inverter converts the DC energy from the solar PV system to AC energy, some energy is lost, which could be due to the cable, PV module, or inverter. As shown in Table 2, this is estimated as inverter percentage conversion loss using equation (2) and the values vary according to the number of energy losses from the inverter given by (3).

$$\text{Inverter percentage conversion loss} = \frac{DC\ Energy - AC\ Energy}{DC\ Energy} \times 100\% \quad (2)$$

$$\eta_{inverter} = \frac{E_{AC}}{E_{DC}} \times 100\% \quad (3)$$

Where: $\eta_{inverter}$ is the inverter efficiency that is the ratio of output energy (AC energy) to input energy (DC energy) multiply by 100%.

C. Yields, Array Capture, and System Losses

Table 3 displays the daily DC array, AC final, and reference yields, DC array capture, and AC system losses of the PV system as measured at quarter-hourly intervals using the ESB Warrenpoint system. These were obtained from the system measurement and analyzed using (4), (5), (6), (7), and (8). In December and May, the monthly daily DC array, AC final, and reference yields, DC array capture, and AC system losses ranged from 0.46 to 4.72 h/day, 0.45 to 4.63 h/day, 5.2 to 16.41 h/day, 4.74 to 11.69 h/day, and 0.01 to 0.09 h/day, respectively. The average annual daily DC array, AC final, and reference yields, DC array capture, and AC system losses were 2.32 hours per day, 2.30 hours per day, 8.83 hours per day, 6.51 hours per day, and 0.02 hours per day, respectively. Figures 7 (a) and 7 (b) show the DC array, AC final, and reference yields of a monthly daily PV system as obtained from the ESB Warrenpoint system, as well as the AC system loss. The DC array capture loss could be due to transient effects (such as shading, dust, wind velocity, ambient temperature, or module temperature) [2], corrosion of solar cell connections, or degradations.

$$Y_{A,day} = \frac{DC\ Energy\ (\frac{kWh}{kWp})}{Total\ number\ of\ days\ in\ operation} \quad (4)$$

$$Y_{F,day} = \frac{AC\ Energy\ (\frac{kWh}{kWp})}{Total\ number\ of\ days\ in\ operation} \quad (5)$$

$$Y_{R,day} = \frac{Solar\ Irradiation\ (\frac{kWh}{m^2})}{\frac{G_{STC}(kWm^2)}{Total\ number\ of\ days\ in\ operation}} \quad (6)$$

$$Lc_{,day} = Y_{R,day} - Y_{A,day} \quad (7)$$

$$Ls_{,day} = Y_{A,day} - Y_{F,day} \quad (8)$$

Where:

- $Y_{A,day}$: daily array yield, that is, the ratio of the DC output energy (kWh) to its module capacity (kW_P) from a solar PV array over a total number of days in operation [22].
- $Y_{F,day}$: daily final yield, that is, the ratio of the AC output energy (kWh) to its module capacity (kWp) from a solar PV array over a total number of days in operation [23].
- $Y_{R,day}$: daily reference yield, that is, the ratio of total daily in-plane solar irradiation (kWh/m^2) its reference solar irradiance (G_{STC}).
- $Lc_{,day}$: daily DC array capture loss, that is, the difference between the DC array yield ($Y_{A,day}$) and the reference yield ($Y_{R,day}$).
- $Ls_{,day}$: daily AC system loss, that is, the difference between the final yield ($Y_{F,day}$) and array yield ($Y_{A,day}$).

DC array yield and AC final yield are plotted as a function of solar irradiance in Figure 8 (a-b) using quarter-hourly (15-minute) interval data. Figure 8 (c-d) shows that the DC array yield and AC final yield are both linearly proportional to solar irradiance. Figure 8 (a-b) depicts sublinear behavior caused by a transient effect like shade/shadow cast, overcast period, or average inverter efficiency loss (about 0.6%) over the PV field. As a result, at low solar irradiance levels, both DC array and AC final yields are either zero or very low due to inverter losses as well as PV generator low irradiance losses.

D. Measurement of Solar Irradiance

Figures 9 and 10 depict various views of the ESB Warrenpoint site solar irradiance, as well as a solar power calendar based on the plane of array solar irradiance averaged for each quarter-hourly period between March and May 2016. March and May were chosen because of their peak clearness indices. It has been observed that March 13, 14, and 22 and May 13, 16, 27, and 31 are clear days, whereas other days such as March 9, 10, 11, 12, 15, 16, 17, 18, and 22, and May 8, 12, 14, 17, 23, 24, 29, and 30 are partly cloudy, and other days such as May 1, 2, 3, 4, 5, 6, 7, 9, 10, 11, 15, 18, 19, 20, 21, 25, 26, and 28, and March 1, 2, 3, 4, 5, 6, 7, 8, 10, 19, 20, 21, 23, 24, 25, 26, 27, 28, 29, 30, and 31 are overcast. As a result of the peak daily clearness index found in May, there are clearer days in May than in March.

E. Measurement of Output Performance

The daily incident solar radiation for any given location is determined by the sun's path across the sky and the amount of cloud cover in the area (Trueblood et al., 2013[46]). Figure 11 (a-d) depicts daytime power profiles at quarter-hourly (15-minute), half-hourly (30-minute), and hourly (60-minute) intervals for three days in each season: a clear day, an overcast day, and a middle day. The clear day, as defined here, is the day of the season with the greatest amount of solar irradiation, resulting in a parabolic curve (see Figure 11 (a-d)); the overcast day is a day with the least amount of solar irradiation, resulting in distortions from perfect parabolic shapes (see Figure 11 (a-d)); and a middle day is a day with the median amount of solar irradiation, resulting in partial parabolic curves. The chosen days of power profiles span the months of each of the four seasons (winter, spring, summer, and autumn) (see Figure 12). Figure 12 shows that the clear days (as seen in Figure 11 (a-d)) in winter, spring, summer, and autumn were caused by an increase in daily sunshine hours in February, May, June, and September. Because of the highest amount of solar irradiation at the site location, these days were generally characterized by an increase in PV output generation. The median increase in daily sunshine hours occur in January, April, July, and October during the winter, spring, summer, and autumn. As a result, PV output generation was moderately high. The overcast day was generally characterized by low solar irradiation due to a decrease in daily sunshine hours, as seen in December, March, August, and November (see Figure 12). As a result, the overcast day generates less PV output. The autumn and winter daily profiles, on the other hand, are more extended, with higher output generation at midday, but they have fewer total hours than the summer and spring profiles, which have more hours of daylength. Because PV panels are more efficient at lower temperatures, output generation is higher during clear days in the spring than during clear days in the summer [24]. The middle day demonstrates that PV output generation can vary throughout the day, owing to cloud movement.

F. Performance Variations

I. Weather-Corrected Performance Ratio (PR)

The performance ratio (PR) is a metric used to evaluate solar photovoltaic installations. PR normalizes the output of the PV system to its installed capacity and the available solar irradiance at the site of installation, allowing a comparison of the performance of systems with different installed capacities in different geographical locations [25]. 3-5 years of data are required to capture seasonal variations [25]. Because the performance ratio is affected by the module and ambient temperature of the system's site location due to variation with changes in meteorological conditions, it is important to measure or quantify this variation and show how it can be removed or reduced by using the two methods described below [26], [27]:

- Traditional calculation of PR (uncorrected PR) using equation (9):

$$PR_{uncorr} = \frac{\sum P_{AC\_t}}{\sum_t [P_{STC}(\frac{G_{POA}}{G_{STC}})]} = PR_{Syst.} = \frac{Y_F}{Y_R} \times 100\% \quad (9)$$

- Modifications of uncorrected PR through temperature normalization to produce a temperature-corrected PR to become a weather-corrected PR using (10):

$$PR_{corr} = \frac{\sum P_{AC\_t}}{\sum_t [P_{STC}(\frac{G_{POA}}{G_{STC}})(1+\frac{\delta}{100}(T_{cell\_avg}-T_{ref}))]} \quad (10)$$

$$R_D = \frac{m \times 12}{c} \times 100\% \quad (11)$$

$$\%T_{Losses} = PR_{uncorrected} - PR_{corrected} \quad (12)$$

Where: PR_{uncorr}: uncorrected performance ratio; PR_{corr}: corrected performance ratio; P_{AC}: measured AC electrical generation (W); P_{STC}: summation of installed modules (49920 W_p);
G_{POA}: measured plane of array (POA) irradiance (W/m^2); t: data collection time (15 mins.); G_{STC}: irradiance at standard test conditions (STC) (1000 W/m^2); T_{ref}: reference temperature (25^{o}C);T_{ref}: reference temperature (25^{o}C); δ : Temperature coefficient for power (-0.4%/^{o}C);
R_D: Degradation rates (%); $\%T_{Losses}$: Percentage temperature losses; m and c are the slope and vertical intercept of the linear trend line of the PR versus time (months) plot respectively.
As a result, the weather-corrected PR from 2016 to 2020 is analyzed using the annual PR regression method, and performance data is

sorted for solar irradiance levels greater than 700 Wm^{-2}, as proposed by Quansah and Adaramola in their works [25]. (11) Is used to compute the degradation rates (R_D) [25].

Figures 13-17 show annual PR regression graphs for five years (2016-2020) for both temperature-corrected PR and uncorrected PR. Table 4 and Figure 18 show the annual uncorrected system PR, temperature-corrected system PR, degradation rates, and percentage of temperature losses from 2016 to 2020. Figure 17 depicts a decrease in PV power output over time due to the performance loss rate or degradation rate. It can be seen using error bars and the Severity ranking of failure mode proposed by Pramod et al [17]. According to Figure 17 and Table 4.

The median degradation rates in 2016 (4.5% /year to 14%/year) and 2017 (0.1% /year to 5.2%/year) are 8.40% /year and 3.87%/year, respectively. This demonstrates that the degradation rate is greater than 1% per year, and the hazardous probability is between 90% and 100%. [17]. This is assigned a severity of 10 (with an associated failure of corrosion in solder bonds) [28] and a severity of 10 (with an associated failure of EVA discoloration) [29].

The median degradation rates in 2018 (-7.5%/year to 2.5%/year), 2019 (-16%/year to -23 %/year), and 2020 (-5.1%/year to -10%/year) are -2.75%/year, -18.23%/year, and -5.2%/year, respectively. This demonstrates that the degradation rates are less than 1%/year and that their hazardous probabilities range from severity rank 9-1 or 80% - 70% to 0% safety hazard [17]. EVA discoloration, metallization of the front side grid, de-lamination between EVA and solar cell, glass weathering, de-lamination between EVA and solar cell, oxidation of antireflecting coating, cell metallization and hotspot, surface soiling, corrosion in solder bond, and de-lamination, junction box degraded could all be associated failures here [17].

CONCLUSIONS

Since environmental factors such as humidity, dust accumulation, and wind velocity are agents of transient and performance loss rates, it is important to minimize or reduce these effects by inspecting the proposed geographical location before the installation of solar PV systems. Because of the diversity of climates, it is essential to broaden the optimization considerations to achieve a more significant result. Instead of using standard methods for installing a solar PV system, it is important to consider dominant factors such as wind directions and speeds, which have transient effects on solar PV system output performance. Since solar cell output performance degrades as cell temperature rises due to thermal degradation, it's critical to maintain the surface of a solar panel at a temperature that doesn't exceed its standard test conditions (25ºC). Air- or water-cooling techniques may help to alleviate the problem of overheating caused by an increase in solar irradiance and high temperatures on a solar panel. Therefore, using the characteristics of an anti-reflecting material to increase the output performance of a solar PV panel is recommended.

Figure 1 (a): Using Bathtub curve to explain PV Durability and Reliability Issues [4].

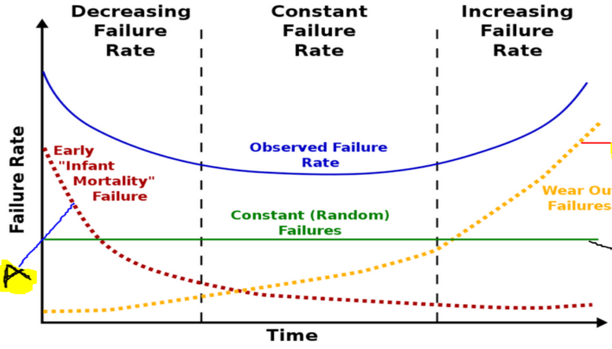

Figure 1 (b): Multiple failure modes overlap of solar PV modules [4].

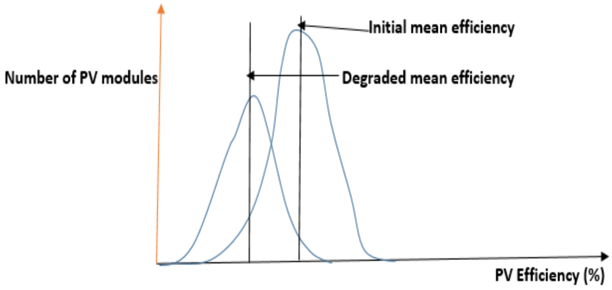

Figure 2: Degradation of Solar PV system [1].

Figure 3: Location and Satellite view of ESB site situated at Upper Dromore Road, Warrenpoint, Northern Ireland, UK (https://www.google.com/maps/place/Newry+BT34+3PN,+UK/@54.1132142,-6.2642131,248a,35y,44.92t/data=!3m1!1e3!4m5!3m4!1s0x4860da664698253b:0xd3507b57cb2eea3!8m2!3d54.1150048!4d-6.2630492).

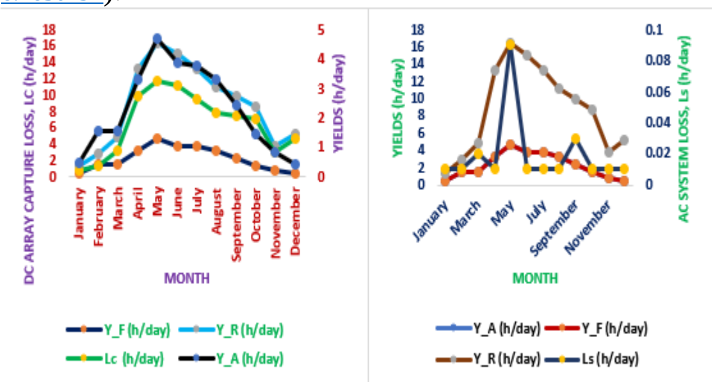

a. b.

Figure 7: Monthly daily yields, DC array capture, and AC system losses of ESB Warrenpoint system.

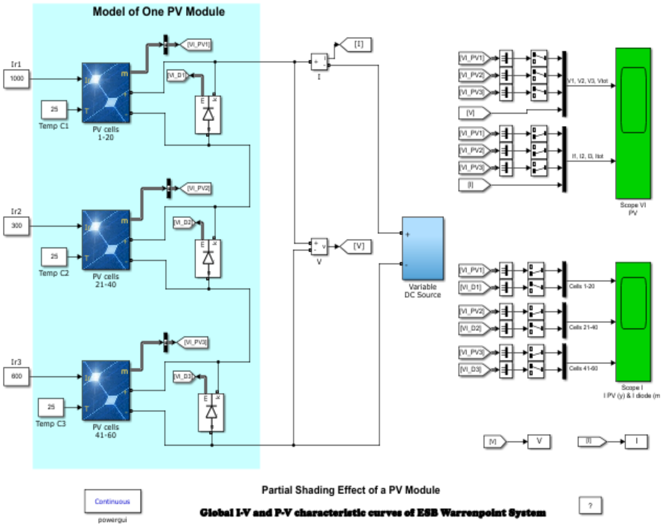

Figure 4: PV module connected to a variable DC voltage source converter (VSC) (https://uk.mathworks.com/help/physmod/sps/ug/partial-shading-of-a-pv-module.html;jsessionid=9479da359d71d0f731ea5a9a6d64)

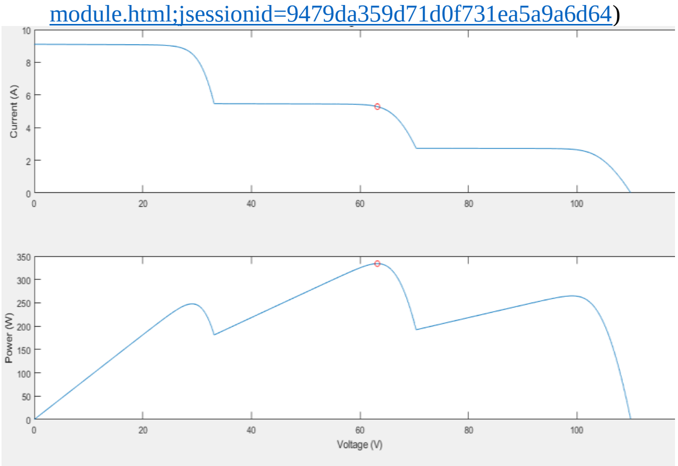

Figure 5: I-V and P-V characteristics curves of a PV system

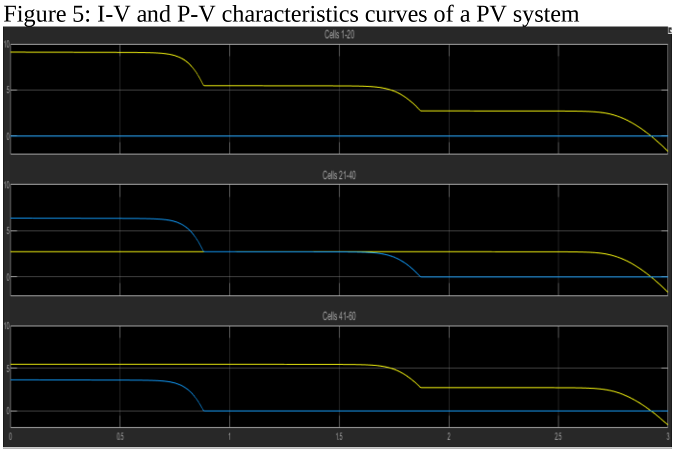

Figure 6: Shading effect of PV current (with yellow color line) and diode current (with blue color).

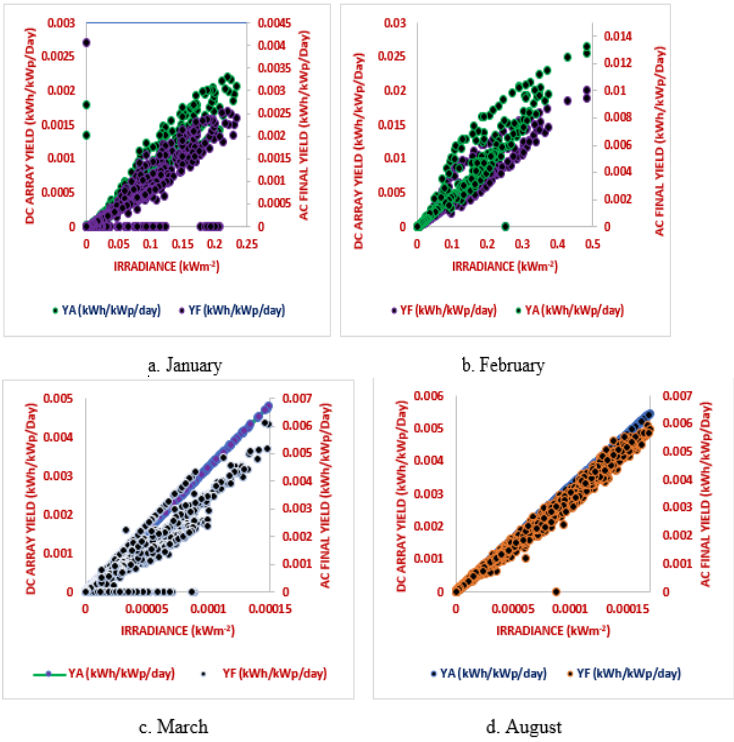

Figure 8: Quarter-Hourly data for AC Final yield and DC Array yield.

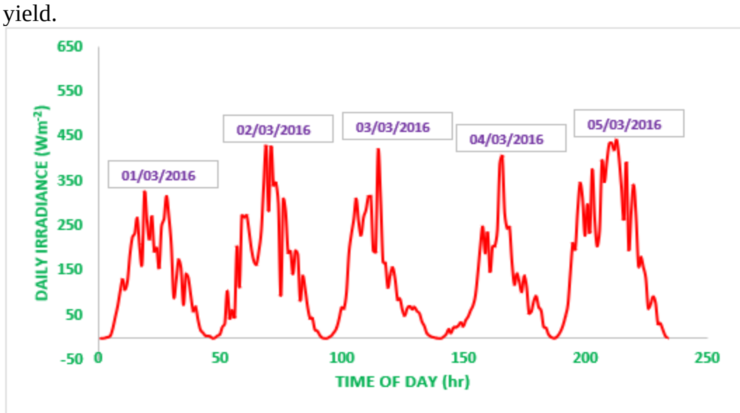

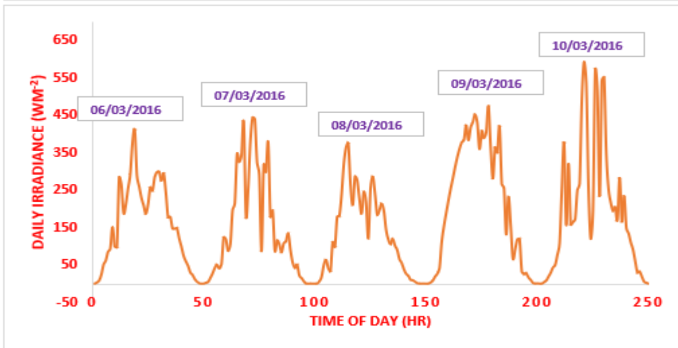

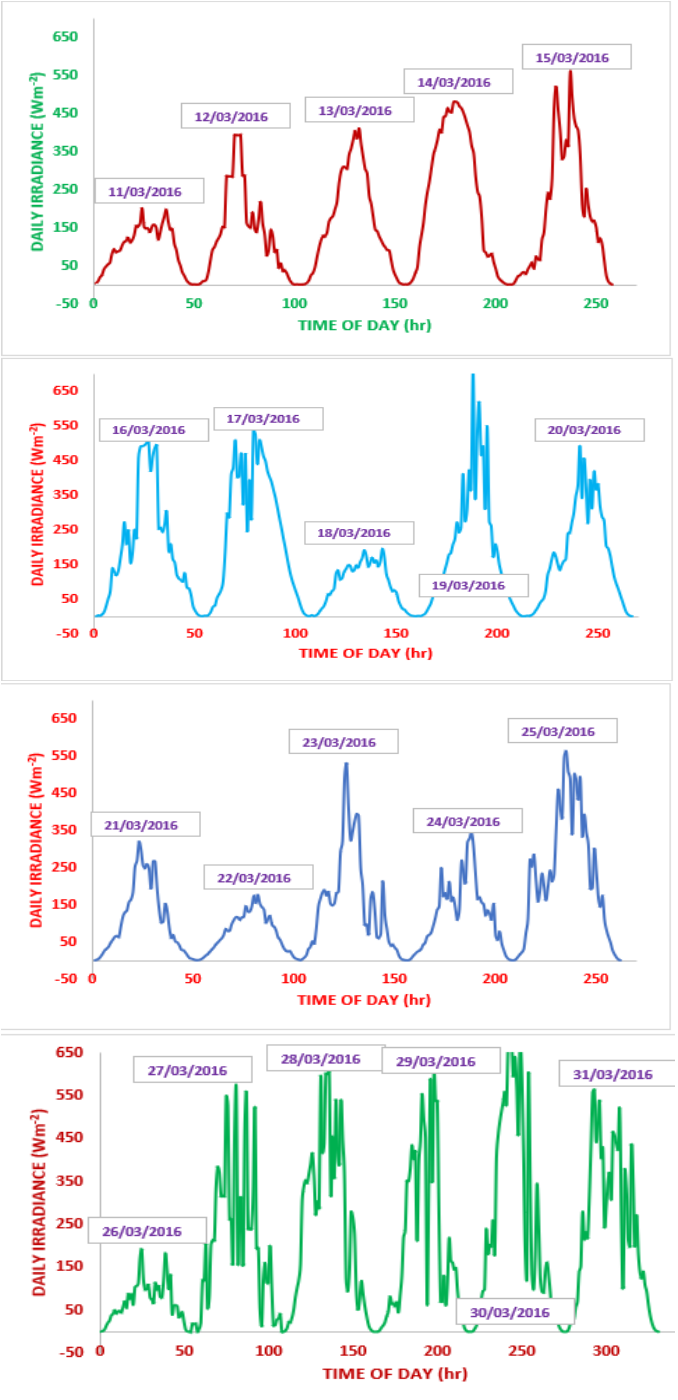

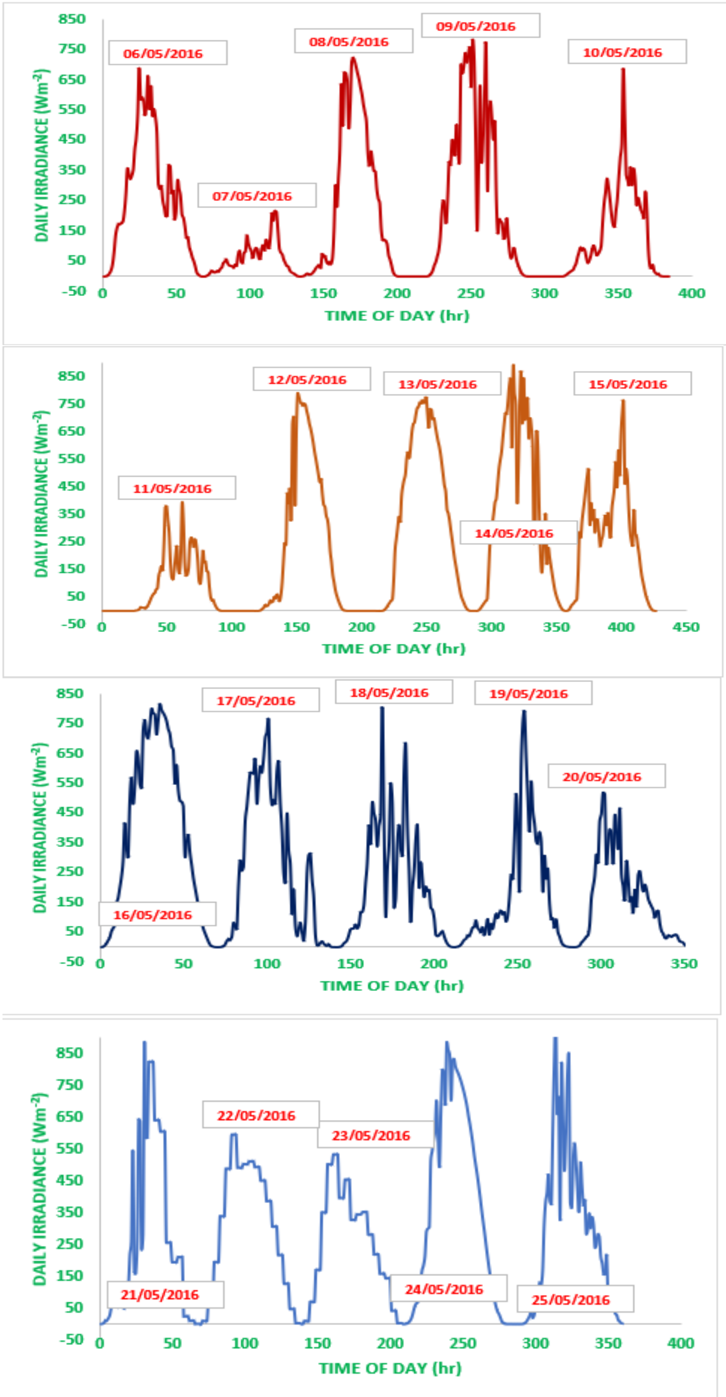

Figure 9: Measured solar irradiance profiles for each day in March 2016.

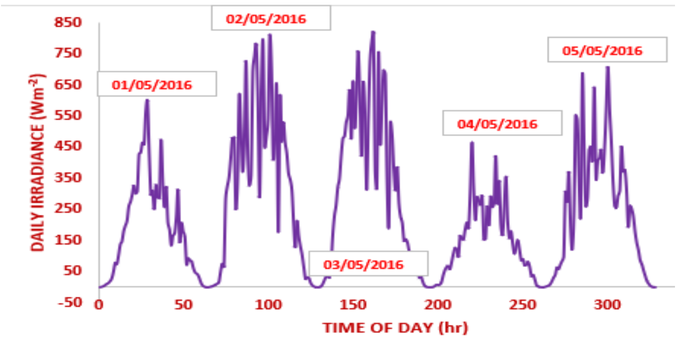

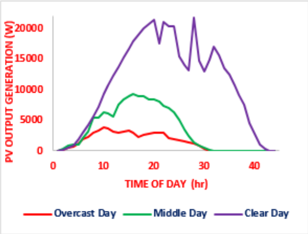

i. Quarter-hourly data for selected days

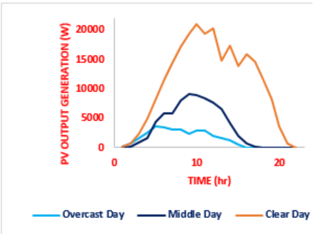

ii. Half-hourly data for selected days

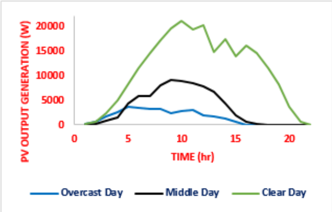

iii. Hourly data for selected days

Figure 11 (a): Power output profiles of selected days during the winter season.

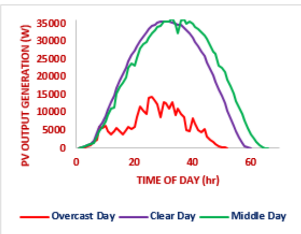

i. Quarter-hourly data for selected days

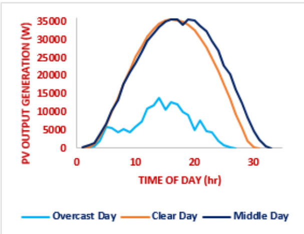

ii. Half-hourly data for selected da

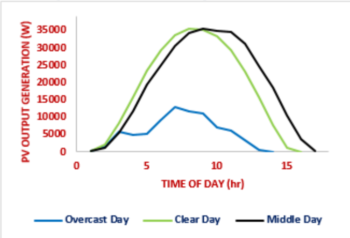

iii. Hourly data for selected days

Figure 11 (b): Power output profiles of selected days during the spring season.

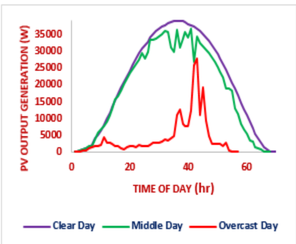

i. Quarter-hourly data for selected days

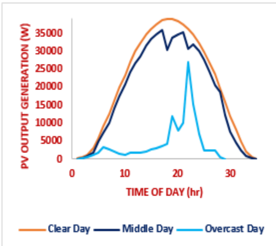

ii. Half-hourly data for selected days

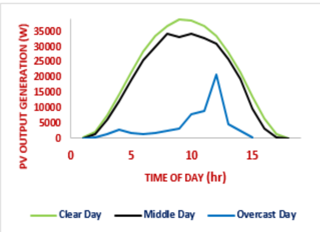

iii. Hourly data for selected days

Figure 11 (c): Power output profiles of selected days during the summer season.

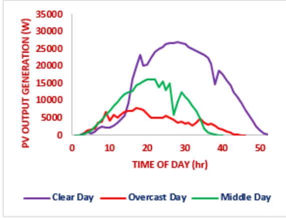

i. Quarter-hourly data for selected days

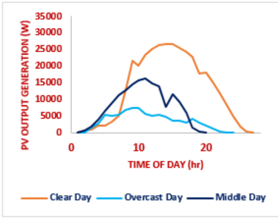

ii. Half-hourly data for selected days

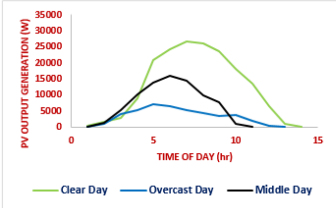

iii. Hourly data for selected days

Figure 11 (d): Power output profiles of selected days during the autumn season.

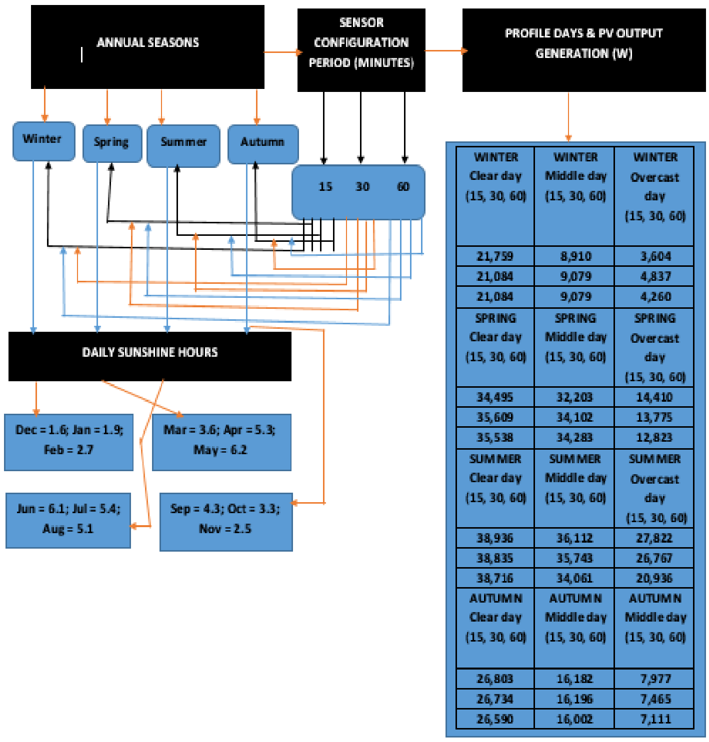

WINTER Clear day (15, 30, 60)	WINTER Middle day (15, 30, 60)	WINTER Overcast day (15, 30, 60)
21,759	8,910	3,604
21,084	9,079	4,837
21,084	9,079	4,260
SPRING Clear day (15, 30, 60)	SPRING Middle day (15, 30, 60)	SPRING Overcast day (15, 30, 60)
34,495	32,203	14,410
35,609	34,102	13,775
35,538	34,283	12,823
SUMMER Clear day (15, 30, 60)	SUMMER Middle day (15, 30, 60)	SUMMER Overcast day (15, 30, 60)
38,936	36,112	27,822
38,835	35,743	26,767
38,716	34,061	20,936
AUTUMN Clear day (15, 30, 60)	AUTUMN Middle day (15, 30, 60)	AUTUMN Middle day (15, 30, 60)
26,803	16,182	7,977
26,734	16,196	7,465
26,590	16,002	7,111

Figure 12: A chart showing power profiles of selected days in winter, spring, summer, and autumn in 15 minutes, 30 minutes, and 60 minutes sensor configuration period of ESB Warrenpoint system.

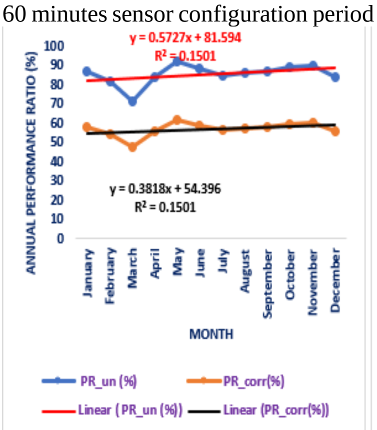

Figure 13: Annual System PR for 2016

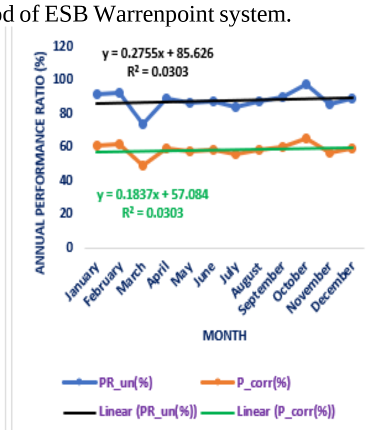

Figure 14: Annual System PR for 2017

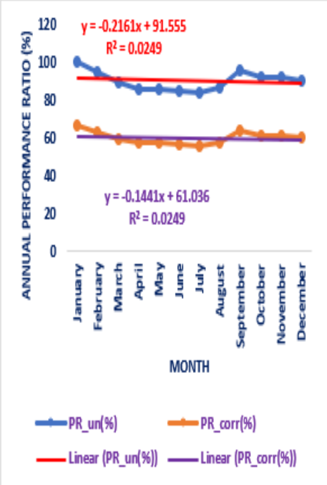

Figure 15: Annual System PR for 2018

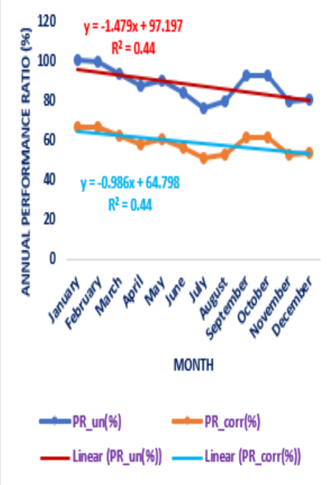

Figure 16: Annual System PR for 2019

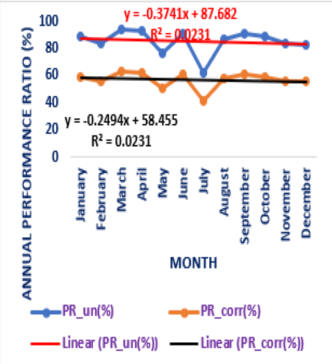

Figure 17: Annual System PR for 2020

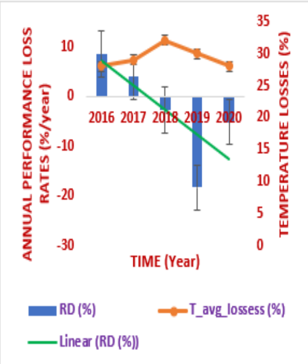

Figure 18: Annual Performance Loss Rates (%/year)

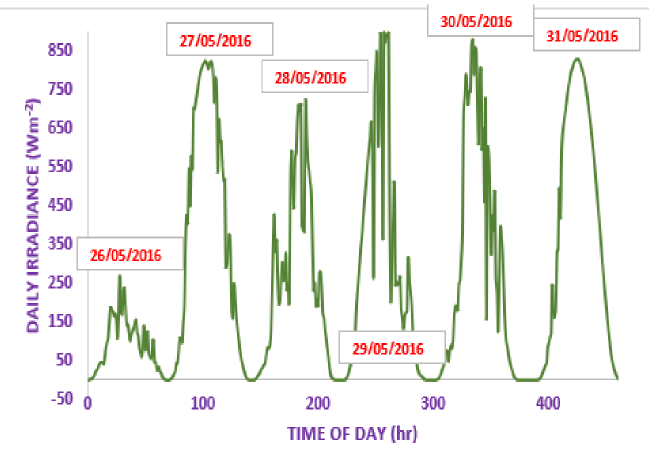

Figure 10: Measured solar irradiance profiles for each day in May 2016.

Table 1: Severity ranking of failure mode [17].

S/N	Severity	Rank
1.	Degradation rate should be >1.0%/year with safety, hazardous probability in the range <90−100>%	10
2.	Degradation rate should be <0.9–1.0>%/year with safety, hazardous probability in the range <80–90>%	9
3.	Degradation rate should be in the range <0.8–0.9>%/year with safety, hazardous probability in the range <70–80>%	8
4.	Degradation rate should be in the range <0.7–0.8>%/year with safety, hazardous probability in the range <60–70>%	7
5.	Degradation rate should be in the range <0.6–0.7>%/year with safety, hazardous probability in the range <50–60%> %	6
6.	Degradation rate should be in the range <0.5–0.6>%/year with safety, hazardous probability in the range <40–50> %	5
7.	Degradation rate should be in the range <0.4–0.5>%/year with safety hazardous probability in the range <30–40>%	4
8.	Degradation rate should be in the range <0.3–0.4>%/year with safety hazardous probability in the range <20–30>%	3
9.	Degradation rate should be in the range <0.2–0.3>%/year with safety hazardous probability in the range <10–20>%/	2
10.	The degradation rate should be <0.1–0.2>%/year with no safety hazard	1

Table 2: Monthly DC Energy and AC Energy, inverter efficiency, and percentage conversion loss of quarter-hourly system measurement obtained from the ESB Warrenpoint System.

Month	DC Energy [MJ]	AC Energy [MJ]	Inverter Efficiency (η) (%)	Inverter Percentage Conversion Loss (%)
January	2763	2720	98.40	1.6
February	1978.6	1975.3	99.80	0.17
March	8640.2	8543.1	98.90	1.12
April	17810.3	17802.16	99.95	0.046
May	26092	25595	98.10	1.51
June	20628	20606.5	99.90	0.104
July	20980	20940	99.81	0.191
August	18320	18291	99.84	0.158
September	12990	12838	98.82	1.17
October	8121	8062	99.27	0.73
November	4540	4531	99.80	0.2
December	2540	2526	99.45	0.55
Total	145,403.1	144,430.1		
Average	12,116.9	12,035.8	99.42	0.629

Table 3: DC array, AC final, and reference yields, DC array capture, and AC system losses of quarter-hourly measured ESB Warrenpoint system.

Month	Y_A (h/day)	Y_F (h/day)	Y_R (h/day)	$Lc_{,day}$ (h/day)	$Ls_{,day}$ (h/day)
January	0.5	0.49	1.39	0.89	0.01
February	1.59	1.58	2.94	1.35	0.01
March	1.56	1.54	4.81	3.25	0.02
April	3.33	3.32	13.31	9.98	0.01
May	4.72	4.63	16.41	11.69	0.09
June	3.86	3.85	15.12	11.26	0.01
July	3.8	3.79	13.31	9.51	0.01
August	3.31	3.3	11.09	7.78	0.01
September	2.43	2.4	9.88	7.45	0.03
October	1.47	1.46	8.66	7.19	0.01
November	0.85	0.84	3.87	3.02	0.01
December	0.46	0.45	5.2	4.74	0.01
Average	2.32	2.30	8.83	6.51	0.02

Table 4: Annual uncorrected system PR, temperature-corrected system PR, degradation rates, and percentage of temperature losses from 2016-2020.

Year	R_D (%/year)	$PR_{uncorrected}$ (%)	$PR_{corrected}$ (%)	$T_{avglosses}$ (%)
2016	4.5 to 14	86.5	58	28.5
2017	0.1 to 5.2	91	61	30
2018	-7.5 to 2.5	99.8	67	32.8
2019	-16 to -23	100	67	33
2020	-5.1 to -10	89	59	30

ACKNOWLEDGMENTS

Our thanks go to the Fiosrai Research Fund of Technological University Dublin, Ireland for funding this research work. We also thank the Electric Supply Board (ESB) of Ireland for permitting us to use data from their solar plant to carry out this research study.

REFERENCES

[1] C.C. Okorieimoh, B. Norton, and M. Conlon, "Long-Term Durability of Solar Photovoltaic Modules" In Scott L., Dastbaz M., Gorse C. (eds) Sustainable Ecological Engineering Design. Springer, Cham, 2020, pp. 317-325. https://doi.org/10.1007/978-3-030-44381-8_24.

[2] C.C. Okorieimoh, B. Norton, and M. Conlon, "Effect of transient performance changes on photovoltaic modules output" Poster. 10TH Annual GRS Symposium, 2019, 10.13140/RG.2.2.28516.94083.

[3] X.Y. Li, "Degradation analysis of photovoltaic modules based on operational data: effects of seasonal pattern and sensor drift", IOP Conf. Series: Earth and Environmental Science, 2016, Vol. 40, pp. 012063. DOI:10.1088/1755-1315/40/1/012063.

[4] F.Z. Allen, and P.D. David, "Photovoltaic Module, Weather Durability and, Reliability" "Will my module last outdoors?". Solar Energy Competence Centre, Atlas Material Testing Technology LLC, 2015. www.atlas-mts.com.

[5] J. Wohlgemuth, "Reliability of PV Systems, Reliability of Photovoltaic Cells, Modules, Components, and Systems", Proc. of SPIE, 2008, Vol. 7048, pp. 704802-1.

[6] Z. Allen, "PV Durability and Reliability Issues. Atlas Material Testing", Journal of Renewable Energy World, 2009, Vol. 1, Issue 5.

[7] E.D. Dunlop, and D. Halton, "The performance of crystalline silicon photovoltaic solar modules after 22 years of continuous outdoor exposure. Prog Photovoltaics", 2006, Vol.14, Issue 1, pp.53–64. DOI: 10.1002/pip.627.

[8] G.N. Tiwari, R.K. Mishra, and S.C.Solanki "Photovoltaic modules and their applications: A review on thermal modeling", Applied Energy, 2011, Vol. 88, pp. 2287-2304.

[9] S. Pingel, O. Frank, M. Winkler, S. Daryan, T. Geipel, H. Hoehne, and J. Berghold, "Potential induced degradation of solar cells and panels", Proc. 35th IEEE Photovolt. Spec. Conf., 2010, pp. pp. 2817-22.

[10] B. Sopori, P. Basnyat, S. Shet, V. Mehta, J. Binns, and J. Appel, "Understanding light-induced degradation of c-Si solar cells", Proc. IEEE Photovolt. Spec. Conf., 2012, pp. 5200-54200.

[11] C.R. Osterwald, A. Anderberg, S. Rummel, and L. Ottoson, "Degradation analysis of weathered crystalline-silicon PV modules," Proc. 29th IEEE Photovolt. Spec. Conf., 2002, pp. 1392-5.

[12] G.N. Tiwari, R.K. Mishra, and S.C. Solanki, "Photovoltaic modules and their applications: A review on thermal modeling", Applied Energy, 2011, Vol. 88, pp.2287-2304.

[13] I. Tetsuyuki, and M. Atsushi, "Annual degradation rates of recent crystalline silicon photovoltaic modules", Progress in photovoltaics: Research and Applications, 2017, Vol. 25, pp. 953-967. DOI: 10.1002/pip.2903.

[14] P. Nochang, J. Jaeseong, and H. Changwoon, "Estimation of the degradation rate of multi-crystalline silicon photovoltaic module under thermal cycling stress. Microelectronics Reliability", 2014. DOI: http://dx.doi.org/10.1016/j.microrel.2014.03.021

[15] M. Saadsaoud, A.H. Ahmeda, Z. Er, and Z. Rouabah, "Experimental study of degradation modes and their effects on the reliability of photovoltaic modules after 12 years of field operation in the steppe region", Special issue of the 3rd International Conference on Computational and Experimental Science and Engineering (ICCESEN 2016), Journal of Acta Physica Polonica A, 2017, Vol. 132, pp.3-11. DOI: 10.12693/APhysPolA.132.930.

[16] H. Takatoshi, N. Tomoya, T. Tadashi, and I. Yoshitaka, "Influence of degradation in units of PV modules on the electric power output of PV system", Journal of International Council on Electrical Engineering, 2018, Vol. 8, No. 1, pp.118–126. DOI: https://doi.org/10.1080/22348972.2018.1477095

[17] R. Pramod, M. Maria, M.K. Nallapaneni, O.S. Sastry, and G.N. Tiwari, "Risk priority number for understanding the severity of photovoltaic failure modes and their impacts on performance degradation," Case Studies in Thermal Engineering, 2019, Vol. 16. https://doi.org/10.1016/j.csite.2019.100563

[18] S. Chattopadhyay, R. Dubey, V. Kuthanazhi, J.J. John, C.S. Solanki, A. Kottantharayil, B.M. Arora, K.L. Narasimhan, V. Kuber, J. Vasi, A. Kumar, and O.S. Sastry, "Visual degradation in field-aged crystalline silicon PV modules in India and correlation With electrical degradation", IEEE J. Photovolt., 2014, Vol 4, pp. 1470-1476.

[19] S. Kumar, S. Roy, and R. Gupta, "Comparison of reliability tests by characterization of degradation in photovoltaic modules", MOJ Sol. Photoenergy Syst., Article 00006, 2017. 10.15406/mojsp.2017.01.00006

[20] D.C. Jordan, T.J. Silverman, J.H. Wohlgemuth, S.R. Kurtz, and K.T. VanSant, "Photovoltaic failure and degradation modes", Prog. Photovolt. Res. Appl., 2017, Vol. 25, pp. 318-326.

[21] J. Kuitche, R. Pan, and G. Tamizhmani, "Investigation of dominant figures modes for field-aged c-Si modules in desert climatic conditions," IEEE J. Photovolt, 2014, Vol. 4, pp. 814-826.
[22] Sustainable Energy Authority of Ireland (SEAI), Irish energy balances: Statistics publications, 1990-2009, Available: www.seai.ie
[23] J.D. Mondol, Y.G. Yohanis, and B. Norton, "The effect of low insolation conditions and inverter oversizing on long-performance of a grid-connected photovoltaic system," Prog. Photovolt. Res. Appl,2006, Vol. 15, pp. 353-368.
[24] C. Trueblood, S. Coley, T. Key, L. Rogers, A. Ellis, C. Hansen, and E. Philplot, "PV measures up for fleet duty, Data from a Tennessee Plant Are Used to Illustrate Metrics That Characterise Plant Performance". DOI: 10.1109/MPE.2012.2234405.
[25] D.A. Quansah, and M.S. Adaramola, "Assessment of early degradation and performance loss in five co-located solar photovoltaic module technologies installed in Ghana using performance ratio time-series regression," Journal of Renewable Energy, 2019, Vol. 131, pp. 900-910.
[26] S. Kurtz, J. Luis Becerra Cruz, E. Riley, and C. Hansen, "Weather-Corrected Performance Ratio," National Renewable Energy Laboratory Technical Report, NREL/TP-5200-57991,2013.
[27] D.C. Jordan, C. Deline, S.R. Kurtz, G.M. Kimball, M. Anderson, "Robust PV Degradation Methodology and Application", IEEE Journal of Photovoltaics, 2018, Vol. 8, pp. 525-531. DOI: 10.1109/JPHOTOV.2017.2779779.
[28] P. Rajput, G.N. Tiwari, B. Bora, and O.S. Sastry, "Visual and electrical degradation of 22 years field age monocrystalline silicon PV module in the composite climate of India", IEEE, 42nd Photovoltaic Specialists Conference (PVSC), 2015, pp. 1-3.
[29] D. Berman, and D. Faiman, "EVA browning and the time-dependence of I-V curve parameters on PV modules with and without mirrors-enhancement in a desert environment", Sol. Energy Mater. Sol. Cells, 1997, Vol. 45, pp. 401-412.